Detecting direction of causal interactions between dynamically coupled signals

Katsuhiko Ishiguro,[1,*] Nobuyuki Otsu,[1,2,†] Max Lungarella,[1,‡] and Yasuo Kuniyoshi[1,§]

[1]*Graduate School of Information Science and Technology, University of Tokyo, 113-8656 Tokyo, Japan*

[2]*National Institute of Advanced Industrial Science and Technology, 305-8568 Tsukuba, Japan*

The problem of temporal localization and directional mapping of the dynamic interdependencies between parts of a complex system is addressed. We present a technique that weights the sampled values so as to minimize the mutual prediction error between pairs of measured signals. The reliability of the detected intermittent causal interactions is maximized by (a) smoothing the weight landscape through regularization, and (b) using a nonlinear (polynomial) variant of the conventional embedding vector. The effectiveness of the proposed technique is demonstrated by studying three numerical examples of dynamically coupled chaotic maps and by comparing it with two other measures of causal dependency.

The identification and quantification of hidden interdependencies between the parts of a complex system promotes a deeper understanding of the system's dynamics. One way of tackling this important but challenging issue is by estimating to what extent a number of carefully selected observables (e.g., pairs of measured signals) are mutually predictive of each other. Causality measures based on this idea have been proposed which quantify the strength and the direction of the causal interaction between bivariate time series (e.g., [1–9]). The basic assumption underlying all these methods is that the causal relationship does not change too rapidly over time. Signals sampled from the real world, however, are rarely stationary and well behaved, and couplings typically appear, disappear, and reappear over time, becoming weaker or growing stronger (e.g., causal interactions between the stock market exchanges of Tokyo and New York). Here, we address the question of how to detect and localize the direction of such temporally intermittent couplings, that is, of how to detect the waxing and waning of causal interactions.

A naive approach is to repeatedly estimate causal relationships within a moving data window of fixed size. In this technique, the moving window slides across the data set in increments of the data interval, and the causal analysis is conducted using the samples contained in the window. The major problem of this approach is how to find an appropriate window size. Too wide a window decreases the temporal resolution of the analysis; too narrow a window reduces the statistical reliability. A less naive technique recently proposed [10] relies on embeddings across multiple realizations of time-dependent dynamics of a system. This technique is quite powerful and can resolve causal relations based on only 200 samples, its major drawback being that it requires at least a few tens of realizations of sample sequences, independently generated from the analyzed system.

The purpose of this paper is to motivate and derive an alternative method for measuring changes in the couplings between interacting systems. To this end, we introduce the notion of a *causality marker*: at each time step the causal interaction is weighted based on its strength. For nonstationary data sets, such weighting is unequal and changes over time as a result of changes in the temporal causal relation between the data. The concept of the causality marker is general and potentially applicable to various existing methods used to detect causal structure [1,5,7,11]. In this paper, we focus on its formulation in the context of Granger causality [4].

For simplicity, we consider the bivariate case. Let $X = \{x_1, x_2, \ldots, x_N\}$ and $Y = \{y_1, y_2, \ldots, y_N\}$ denote two simultaneously measured time series each consisting of N scalar quantities. As in most previous approaches, we start by reconstructing the state spaces corresponding to both time series by the method of time delay embedding, in which the state (or embedding) vectors are formed by delayed past scalar observations of the time series [12]. The embedding vector of dimension m of X is $\boldsymbol{x}_t^{m,d} = (x_t, x_{t-d}, x_{t-2d}, \ldots, x_{t-(m-1)d})^T$, where d is the time delay (or lag) between successive elements of the vector. If not otherwise stated, in this paper $d=1$, and we use the expression $\boldsymbol{x}_t = (x_t, x_{t-1}, x_{t-2}, \ldots, x_{t-m+1})^T$. Similarly, we define $\boldsymbol{y}_t$. For the choice of adequate values for m and d, we refer to [13,14].

The notion of Granger causality between two time series is based on the idea that the prediction of one time series through linear autoregression can be improved by incorporating information about the past values of the other time series. To estimate the causal effect of $Y \Rightarrow X$ (dependency of X on Y), the two following autoregression equations are used:

$$x_{t+1} = \boldsymbol{\alpha}^T \boldsymbol{x}_t + \pi + \epsilon_t^{(x)}, \tag{1}$$

$$x_{t+1} = \boldsymbol{a}^T \boldsymbol{x}_t + \boldsymbol{b}^T \boldsymbol{y}_t + p + \epsilon_t^{(x|y)}, \tag{2}$$

where the terms $\boldsymbol{\alpha}$, π, $\boldsymbol{a}$, $\boldsymbol{b}$, and p are determined so as to minimize the variance of the prediction errors $\epsilon_t^{(x)}$ and $\epsilon_t^{(x|y)}$,

---

*Corresponding author. Present address: NTT Communication Science Laboratories, 619-0237 Kyoto, Japan. ishiguro@cslab.kecl.ntt.co.jp

†otsu.n@aist.go.jp

‡Present address: Artificial Intelligence Laboratory, University of Zurich, Zurich, Switzerland. lunga@ifi.uzh.ch

§kuniyosh@isi.imi.i.u-tokyo.ac.jp

$$\min_{\boldsymbol{\alpha},\boldsymbol{\pi}}\frac{1}{N}\sum_t (\epsilon_t^{(x)} - \eta^{(x)})^2, \tag{3}$$

$$\min_{\boldsymbol{a},\boldsymbol{b},\boldsymbol{p}}\frac{1}{N}\sum_t (\epsilon_t^{(x|y)} - \eta^{(x|y)})^2, \tag{4}$$

with η denoting the time-averaged error. After calculating the coefficients, we can express the Granger causality as

$$C_{Y\Rightarrow X} = 1 - \frac{\mathrm{var}(\epsilon_t^{(x|y)})}{\mathrm{var}(\epsilon_t^{(x)})} = 1 - \frac{\displaystyle\sum_t (\epsilon_t^{(x|y)} - \eta^{(x|y)})^2}{\displaystyle\sum_t (\epsilon_t^{(x)} - \eta^{(x)})^2}.$$

Intuitively, the larger $C_{Y\Rightarrow X}$ the more X is causally dependent on Y. The dependence in the opposite direction, $C_{X\Rightarrow Y}$, can be defined in a similar way.

The idea of the causality marker is based on the assumption that, for improving the detection of causal relationships, the analysis should place more emphasis (weight) on observables having a larger causal influence on other observables. This weight, called the causality marker, should be large if a causal dependency exists, but should take a small value otherwise. In other words, causality markers indicate ("mark") the locations of potential causal relationships.

Given two bivariate time series X and Y consisting of N samples, we define as causality markers the two N-dimensional weight vectors $W_{X\Rightarrow Y}=\{w_t^{x\to y}\}$ and $W_{Y\Rightarrow X}=\{w_t^{y\to x}\}$ for which $\sum_t w_t^{x\to y}=\sum_t w_t^{y\to x}=N$, $w_t^{x\to y}\geq 0$, and $w_t^{y\to x}\geq 0$. Using these weight vectors, we can reformulate Eqs. (3) and (4) as

$$\min_{\boldsymbol{\alpha},\boldsymbol{\pi}}\frac{1}{N}\sum_t w_t^{y\to x}(\epsilon_t^{(x)} - \eta^{(x)})^2, \tag{5}$$

$$\min_{\boldsymbol{a},\boldsymbol{b},\boldsymbol{p}}\frac{1}{N}\sum_t w_t^{y\to x}(\epsilon_t^{(x|y)} - \eta^{(x|y)})^2. \tag{6}$$

What one seeks are two sets of weights $\{w_t^{x\to y}\}$ and $\{w_t^{y\to x}\}$ that maximize $C_{X\Rightarrow Y}$ and $C_{Y\Rightarrow X}$. These weights can be calculated by substituting the results of Eqs. (5) and (6) in the following "weighted" Granger causality measure:

$$\max_{W_{Y\Rightarrow X}} C_{Y\Rightarrow X} = \max_{W_{Y\Rightarrow X}}\left(1 - \frac{\displaystyle\sum_t w_t^{y\to x}(\epsilon_t^{(x|y)} - \eta_t^{(x|y)})^2}{\displaystyle\sum_t w_t^{y\to x}(\epsilon_t^{(x)} - \eta_t^{(x)})^2}\right). \tag{7}$$

Analogous expressions exist for $C_{X\Rightarrow Y}$ and $W_{X\Rightarrow Y}$.

Although this maximization problem cannot be solved analytically, it is possible to analytically derive the partial derivatives of C with respect to W, and numerically determine the local maximum through the method of steepest descent.

Our method has several interesting properties. First, it does not rely on parameters such as window size or the amount of overlap between adjacent windows, as is the case for the moving window technique. Second, the number of processed samples is not limited to the ones contained in a

particular window centered at a specific time step. The absence of windowing enables us to avoid the dilemma between statistical reliability and granularity of analysis caused by an inadequate window size.

One major drawback of the analysis based on causality markers is the irregularities (roughness) originating from the application of the steepest descent algorithm (which computes a gradient). The causality marker is calculated locally based on the improvement of the regression at each time step, making the estimation dependent on the quality of the observed values. This property is not desirable if the method is applied to data sampled from chaotic systems, which in the general case can display rather complex dynamics, or to data collected from real world systems, which are typically contaminated by noise or inconsistencies. An interesting denoising technique for noisy bivariate data sets relying on Kalman filtering was recently proposed in [15]. This technique, however, assumes that the time series are generated from a system with stationary dynamics, and not characterized by temporally intermittent couplings.

We cope with both issues by penalizing Eq. (7) with a regularization term

$$\max_{W_{Y\Rightarrow X}}\left(C_{Y\Rightarrow X} + \lambda \frac{\frac{1}{N}\sum_t (w_t^{y\to x} - \bar{w})^2}{\frac{1}{N}\sum_t \sigma^2(t)}\right), \tag{8}$$

where

$$\sigma^2(t) = \frac{1}{2l+1}\sum_{i=-l}^{l}\left(w_{t+i}^{y\to x} - \frac{1}{2l+1}\sum_{j=-l}^{l} w_{t+j}^{y\to x}\right)^2,$$

$\bar{w}$ is the average of the causality markers over all time steps, $\lambda\geq 0$ controls the effectiveness of the regularizing second term, and l is the size of the window used to calculate the "local" variance $\sigma^2(t)$ (in all our experiments, $l=2$). To maximize Eq. (8), it is necessary to maximize $C_{Y\Rightarrow X}$ as well as its second term. To achieve this, the denominator $\sigma^2(t)$ should be small and the numerator ("global" variance) should be large. By satisfying these two requirements, the causality marker is "smoothed" and the difference of coupling strength between the weakly and strongly causally related periods is widened, keeping the global variance large. In this paper, we optimize λ to yield the best results in our experiments. There is no decisive approach, however, for the choice of λ if no validation information is provided.

To more effectively handle data with nonlinear dynamics, we use a polynomial embedding vector (PEV) [11,16]. The PEV consists of the polynomial combinations of the monomial components of $\boldsymbol{x}_t$, namely, $\tilde{x}_t(i,j,R)=\prod_{k=i}^{j} x_{t-k}^{R_k}$, where $0\leq i\leq j<m$, $R_k\geq 0$, and $1\leq \sum_{k=i}^{j} R_k\leq R$. By arranging all $\tilde{x}_t(i,j,R)$ in an array, we can define the PEV as $\tilde{\boldsymbol{x}}_t\triangleq(x_t,\ldots,x_{t-m+1},x_t^2,x_t x_{t-1},\ldots,x_{t-m+1}^R)^T$. We define $\tilde{\boldsymbol{y}}_t$ analogously. PEV-based Granger causality (PEVGC) extends Granger causality by replacing $\boldsymbol{x}_t$ with $\tilde{\boldsymbol{x}}_t$ and $\boldsymbol{y}_t$ with $\tilde{\boldsymbol{y}}_t$ in Eqs. (1) and (2). Instead of $\boldsymbol{x}_t$ and $\boldsymbol{y}_t$, in Eq. (2) we can also employ a joint-state PEV $\tilde{\boldsymbol{z}}_t$, derived from $\boldsymbol{z}_t=(\boldsymbol{x}_t^T \boldsymbol{y}_t^T)^T$. Such a joint-state PEV has been recently applied to the analysis of

TABLE I. Coupling strength parameters for artificial data sets.

Time step	Hénon		Sine-based	
	e_{yx}	e_{xy}	e_{yx}	e_{xy}
0–300	0.0	0.0	0.0	0.0
300–600	0.0	0.5	0.0	0.7
600–900	0.5	0.5	0.7	0.0
900–1200	0.0	0.0	0.0	0.0
1200–1500	0.0	0.25	0.35	0.7

the dynamics of climatic modes [16]. Selecting R is also not an easy problem, but in general a small value of R (0–3) is sufficient and preferable. There are two reasons for choosing a smaller value of R: one is that higher-order correlations are not effective for regression in many cases because of the volatility, and the other is that larger R reduces computational efficiency exponentially.

To illustrate the performance of the proposed technique, we analyzed the bivariate time series extracted from three dynamical systems and compared the results with two other approaches: (i) a combination of a moving window analysis and naive (linear) Granger causality; (ii) a combination of a moving window analysis and PEVGC. In what follows, we will show that the causality-marker-based method outperforms the other two.

The first system of interest was composed of two bidirectionally coupled identical Hénon maps
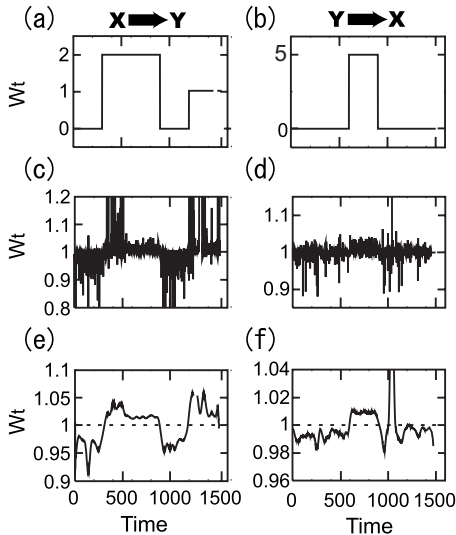

FIG. 1. Expected (true) and estimated coupling directions (causality markers) for coupled Hénon maps. The horizontal axis denotes time; the vertical axis represents the value of the markers $W_{X⇒Y}$ (left) and $W_{Y⇒X}$ (right). The dotted lines represent the threshold values. (a),(b) Expected (true) coupling: (a) X⇒Y and (b) Y⇒X. (c),(d) Estimated coupling without regularization ($\lambda=0.0$): (c) X⇒Y and (d) Y⇒X. (e),(f) Estimated coupling with regularization ($\lambda=10.0$): (e) X⇒Y and (f) Y⇒X.
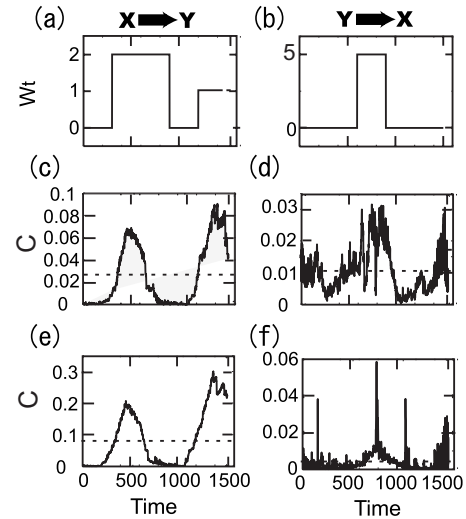

FIG. 2. Moving window analysis of temporal causality measures for coupled Hénon maps. The horizontal axis denotes time; the vertical axis represents the value of the measures $C_{X⇒Y}$ (left) and $C_{Y⇒X}$ (right). The dotted lines represent the threshold values. (a),(b) Expected (true) coupling borrowed from Fig. 1: (a) X⇒Y and (b) Y⇒X. (c),(d) Estimated causality measures with naive Granger causality: (c) X⇒Y and (d) Y⇒X. (e),(f) Estimated causality measures with PEVGC: (e) X⇒Y and (f) Y⇒X.

$$x_{t+1} = 1.4 - [e_{yx}y_t + (1 - e_{yx})x_t]x_t + 0.3x_{t-1},$$

$$y_{t+1} = 1.4 - [e_{xy}x_t + (1 - e_{xy})y_t]y_t + 0.3y_{t-1},$$

where e_{xy} and e_{yx} denote the coupling strengths of x_t on y_t and y_t on x_t, respectively. After discarding 10^4 samples as transients, we collected $N=1500$ samples while the coupling strengths were altered according to Table I. Due to the sudden changes of the coupling constants, the extracted bivariate data were rendered manifestly nonstationary. The embedding dimension m and order R of the PEV were optimized in sample to yield the best result, and were set to $m=3$ and $R=2$, respectively. All causality markers were initialized to 1, and the steepest descent algorithm maximizing $C_{X⇒Y}$ and $C_{Y⇒X}$ was iterated 20 times to yield the estimated couplings between the time series. To eliminate edge effects, we cut off the last few causality marker values. We show the results in Fig. 1. As shown in Figs. 1(e) and 1(f), the regularized causality markers are sufficiently similar to the expected ones [Figs. 1(a) and 1(b)]. The smoothing effect of the regularization term is also noteworthy.

For a comparison, we present the results of a moving window analysis with naive and PEV Granger causality. To estimate the amount of causal interaction, a moving window of 300 samples was slid across the time axis one time step at a time, and the causality measures were evaluated for every window. The estimated couplings are shown in Fig. 2. As evident from the figures, each method [Figs. 2(c) and 2(d) for naive Granger causality, and Figs. 2(e) and 2(f) for PEVGC] fails to detect the X⇒Y couplings in the interval $t=600-900$. The limited sample size makes true directional coupling Y⇒X difficult to estimate. We can also observe
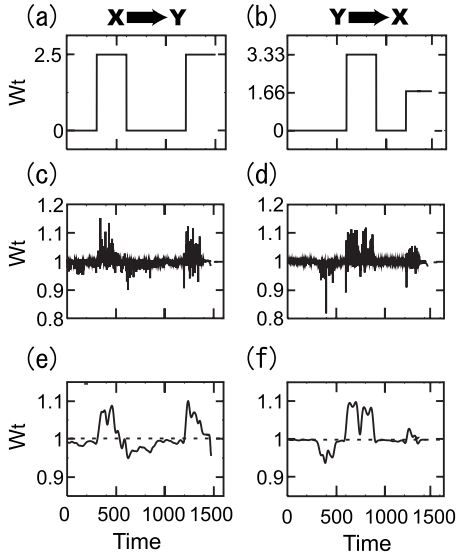
FIG. 3. Expected (true) and estimated coupling directions (causality markers) for coupled sine-based chaotic maps. The horizontal axis denotes time; the vertical axis represents the value of the markers $W_{X \Rightarrow Y}$ (left) and $W_{Y \Rightarrow X}$ (right). The dotted lines represent the threshold values. (a),(b) Expected (true) coupling: (a) $X \Rightarrow Y$ and (b) $Y \Rightarrow X$. (c),(d) Estimated coupling without regularization ($\lambda = 0.0$): (c) $X \Rightarrow Y$ and (d) $Y \Rightarrow X$. (e),(f) Estimated coupling with regularization ($\lambda = 10.0$): (e) $X \Rightarrow Y$ and (f) $Y \Rightarrow X$.

that, by contrast with the causality-marker-based method, the other two measures are characterized by more gentle trends.

In our second numerical experiment, we studied a sine-based chaotic map
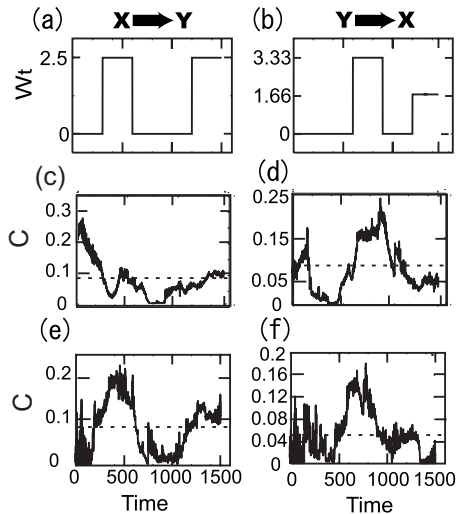

FIG. 4. Moving window analysis of temporal causality measures for sine-based chaotic maps. The horizontal axis denotes time; the vertical axis represents the value of the measures $C_{X \Rightarrow Y}$ (left) and $C_{Y \Rightarrow X}$ (right). The dotted lines represent the threshold values. (a),(b) Expected (true) coupling borrowed from Fig. 3: (a) $X \Rightarrow Y$ and (b) $Y \Rightarrow X$. (c),(d) Estimated causality measures with naive Granger causality: (c) $X \Rightarrow Y$ and (d) $Y \Rightarrow X$. (e),(f) Estimated causality measures with PEVGC: (e) $X \Rightarrow Y$ and (f) $Y \Rightarrow X$.
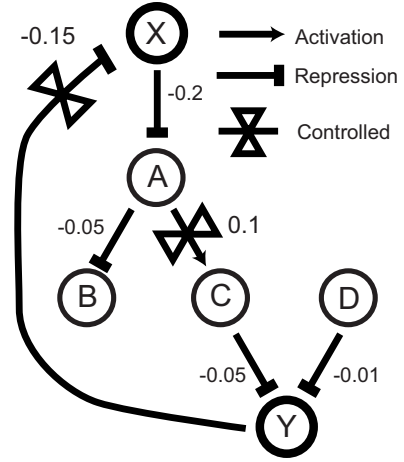

FIG. 5. Studied gene regulatory network structure. The network consists of six nodes; the time series are extracted from nodes X and Y. The numbers labeling the lines are the strength of excitory (>0) or inhibitory (<0) connections.

$$x_{t+1} = 1.7 - 0.4x_t^2 + 1.1 \sin(x_{t-1} - e_{yx}y_{t-1}),$$

$$y_{t+1} = 1.7 - 0.4y_t^2 + 1.1 \sin(y_{t-1} - e_{xy}x_{t-1}).$$

All parameters were the same as in the previous experiment, except for the coupling strengths (Table I) and the PEV order ($R=3$). The coupling constants (e_{xy} and e_{yx}) were varied according to the pattern shown in Figs. 3(a) and 3(b). As can be observed in Fig. 3, despite the peakiness of the curves, the causal dependency between the two maps is well reflected for the $X \Rightarrow Y$ relationship [Figs. 3(c) and 3(e)]. For the case of $Y \Rightarrow X$ [Figs. 3(d) and 3(f)], the calculated causality markers for $t=1200$–1500 are relatively small. It is known that for this map for $e < 0.5$ the detection of the coupling is nontrivial [11].

As in the previous experiment, here also we present the results of a moving window analysis with naive and PEV Granger causality. The width of the moving window was 300 samples. The estimated coupling constants are shown in Fig. 4. As evident from the figure, the obtained causality measures are less similar to the true coupling status.

In our third experiment, we tested the proposed causality marker with time series extracted from a genetic regulatory network model [17]. The studied network is depicted in Fig. 5. The network has several nodes ("genes") linked by weighted connections. The connections are directional and

TABLE II. Coupling strength parameters for gene regulatory network data.

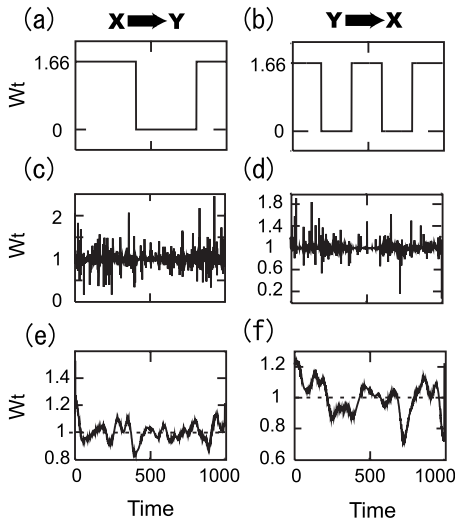| Time step	$Y \rightarrow X (H_{xy})$	$X \rightarrow Y (H_{yx})$
0–200	−0.15	0.1
200–400	0.0	0.1
400–600	−0.15	0.0
600–800	0.0	0.0
800–1000	−0.15	0.1

FIG. 6. Expected (true) and estimated coupling directions (causality markers) for gene regulatory network data. The horizontal axis denotes time; the vertical axis represents the value of the markers: $W_{X \Rightarrow Y}$ (left) and $W_{Y \Rightarrow X}$ (right). The dotted lines represent the threshold values. (a),(b) Expected (true) coupling: (a) $X \Rightarrow Y$ and (b) $Y \Rightarrow X$. (c),(d) Estimated coupling without regularization ($\lambda = 0.0$): (c) $X \Rightarrow Y$ and (d) $Y \Rightarrow X$. (e),(f) Estimated coupling with regularization ($\lambda = 10.0$): (e) $X \Rightarrow Y$ and (f) $Y \Rightarrow X$.

have weights as shown in the figure. All the connections are inhibitory except the one between the nodes A and C, which is excitatory. Specifically, in our experiments we controlled two connection weights to realize temporal changes in the causal relationships between the nodes X and Y. The connection weight between the nodes Y and X can be understood as
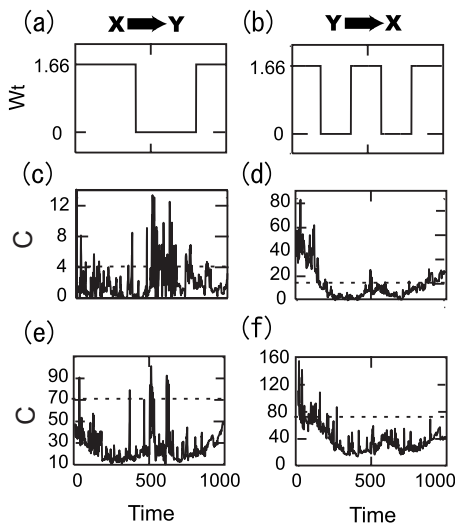

FIG. 7. Moving window analysis of temporal causality measures for gene regulatory network data. The horizontal axis denotes time; the vertical axis represents the value of the measures $C_{X \Rightarrow Y}$ (left) and $C_{Y \Rightarrow X}$ (right). The dotted lines represent the threshold values. (a),(b) Expected (true) coupling borrowed from Fig. 6: (a) $X \Rightarrow Y$ and (b) $Y \Rightarrow X$. (c),(d) Estimated causality measures with naive Granger causality: (c) $X \Rightarrow Y$ and (d) $Y \Rightarrow X$. (e),(f) Estimated causality measures with PEVGC: (e) $X \Rightarrow Y$ and (f) $Y \Rightarrow X$.
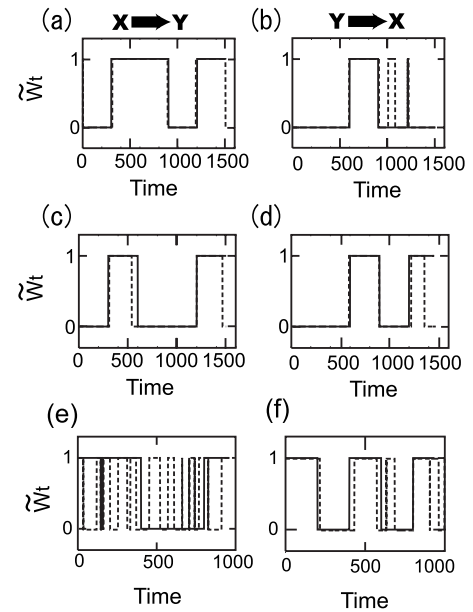

FIG. 8. Binary classified causality markers. Solid lines denote the classification results of expected causality markers $\hat{W}_{X \Rightarrow Y}$ (left) and $\hat{W}_{Y \Rightarrow X}$ (right). Dashed lines represent the classification results of estimated causality markers $\tilde{W}_{X \Rightarrow Y}$ (left) and $\tilde{W}_{Y \Rightarrow X}$ (right). (a),(b) Results of analysis on Hénon map data ($\lambda = 10.0$): (a) $X \Rightarrow Y$ and (b) $Y \Rightarrow X$. (c),(d) Results of analysis on sine-based chaotic map data ($\lambda = 10.0$): (c) $X \Rightarrow Y$ and (d) $Y \Rightarrow X$. (e),(f) Results of analysis on gene regulatory network data ($\lambda = 10.0$): (e) $X \Rightarrow Y$ and (f) $Y \Rightarrow X$.

the strength of the $Y \Rightarrow X$ causal relation; whereas the one between the nodes A and C is used as an indicator of the $X \Rightarrow Y$ causal relationship. The $X \Rightarrow Y$ link between A and C does not directly connect X and Y. We thus assume that the causal relationship in the $X \Rightarrow Y$ direction is more difficult to detect.

The expression levels of all M nodes composing the network are described as [17] $g_{t+1} = g_t + H(g_t - \Gamma) + \epsilon$, where g_t^i is the expression level of the ith gene, H is a connectivity strength matrix whose elements are zero except for the designated connections in Fig. 5, Γ is a constant vector whose elements are all set to 50, and ϵ is a uniform noise drawn from $[-10, 10]$. A ceiling function is used to truncate the values of g_t^i at 0 for the lowest and 100 for the largest, yielding signals with highly nonlinear properties. We collected gene expression values for 1000 time steps, and estimated the causal relationship between the nodes X and Y. The coupling strengths H_{xy} and H_{yx} are presented in Table II. We selected the embedding dimension $m = 2$ and $R = 3$. Experimental results are presented in Fig. 6 for the causality marker

TABLE III. Misclassification rates for Hénon map data set.

Method	$X \Rightarrow Y$	$Y \Rightarrow X$
Moving window+naive GC	0.2127	0.2487
Moving window+PEVGC	0.2300	0.1767
Causality marker+PEVGC	0.0227	0.0647

TABLE IV. Misclassification rates for sine-based map data set.

Method	$X{\Rightarrow}Y$	$Y{\Rightarrow}X$
Moving window+naive GC	0.3873	0.4627
Moving window+PEVGC	0.1207	0.3453
Causality marker+PEVGC	0.0727	0.118

TABLE V. Misclassification rates for gene regulatory network.

Method	$X{\Rightarrow}Y$	$Y{\Rightarrow}X$
Moving window+naive GC	0.6660	0.2910
Moving window+PEVGC	0.4330	0.3200
Causality marker+PEVGC	0.417	0.17

based approach and in Fig. 7 for the moving window analysis with a window size of 200 samples. The detection of the $X{\Rightarrow}Y$ coupling is difficult and fails for all methods. However, the causality marker performs better in estimating the $Y{\Rightarrow}X$ causal relationship than the moving window method.

To obtain a better estimate of the coupling direction, the resulting causality markers [Figs. 1(e), 1(f), 3(e), 3(f), 6(e), and 6(f)] were partitioned into two classes by applying the following classification rule (thresholded with the average value of w_t):

$$w_t \Rightarrow \begin{cases} \widetilde{w}_t = 1 & \text{if } w_t \geq 1 \text{ (causally related)}, \\ \widetilde{w}_t = 0 & \text{if } w_t < 1 \text{ (causally unrelated)}. \end{cases} \quad (9)$$

By comparing the classification results $\widetilde{W}_{X{\Rightarrow}Y}$ and $\widetilde{W}_{Y{\Rightarrow}X}$ with the classification results of the expected causality markers [Figs. 1(a), 1(b), 3(a), 3(b), 6(a), and 6(b)], we can compute the misclassification rate with $P=\Sigma_t \|\widetilde{w}_t - \hat{w}_t\|/N$ where $\hat{w}_t$ is the "true" classification result, and N is the number of samples. The classified causality markers for all data sets are shown in Fig. 8 and the misclassification rates are reproduced in Tables III–V. The misclassification rates for the moving window analysis are calculated analogously. At each time step (window), the computed causality measure is thresholded by the average of causality measures of all the windows. The comparison with the moving window analysis reveals that the misclassificaation rates of causality markers are quite satisfactory.

In conclusion, we addressed an important issue in the context of complex dynamical systems analysis, that is, the assessment of dynamic interdependencies between the constituent parts of a complex system based on measured variables. To automatically localize and map the direction of such dependencies, we proposed the notion of causality marker, which evaluates the strength of the causal relationship at every time step rather than an average throughout all time steps. The advantages of our approach are twofold: (a) it is bottom up, that is, there is no need for *a priori* assumptions on the analyzed data or on the employed causality measure; (b) it can be easily applied to all nonlinear extensions of Granger causality—at least to the ones known to the authors [1,7,11,18]. Our experimental results show that our method in combination with nonlinear extended Granger causality and a simple classifier is able to detect changes in the coupling between two interacting system with a high temporal resolution. As one of the directions for further study, we mention a formulation of the causality marker applicable to other measures of causal dependency, such as probabilistic and information-theoretic approaches (e.g., [6]). We point out that, in contrast to the iterative (batch) calculations of the steepest descent, an incremental variant of the causality marker algorithm might be particularly beneficial for very long time series data. We finally note that large-dimensional or continuous-time problems remain an open issue, and that our experiments serve only the purpose of demonstrating the potential of the proposed method.

[1] N. Ancona, D. Marinazzo, and S. Stramaglia, Phys. Rev. E **70**, 056221 (2004).
[2] J. Arnhold, P. Grassberger, K. Lehnertz, and C. E. Elger, Physica D **134**, 419 (1999).
[3] U. Feldmann and J. Bhattacharya, Int. J. Bifurcation Chaos Appl. Sci. Eng. **14**, 505 (2004).
[4] C. W. J. Granger, Econometrica **37**, 424 (1969).
[5] M. Lungarella, K. Ishiguro, Y. Kuniyoshi, and N. Otsu, Int. J. Bifurcation Chaos Appl. Aci. Eng. **17**, 903 (2007).
[6] T. Schreiber, Phys. Rev. Lett. **85**, 461 (2000).
[7] D. Marinazzo, M. Pellicoro, and S. Stramaglia, Phys. Rev. E **73**, 066216 (2006).
[8] M. G. Rosenblum and A. S. Pikovsky, Phys. Rev. E **65**, 041909 (2002).
[9] D. A. Smirnov and B. P. Bezruchko, Phys. Rev. E **68**, 046209 (2003).
[10] R. Andrzejak, A. Ledberg, and G. Deco, New J. Phys. **8**, 6 (2006).
[11] K. Ishiguro, N. Otsu, M. Lungarella, and Y. Kuniyoshi, Phys. Rev. E (to be published).
[12] M. Takens, in *Dynamical Systems and Turbulence*, edited by D. Rand and L. Young, Lecture Notes in Mathematics Vol. 898 (Springer-Verlag, Berlin, 1981), pp. 366–381.
[13] M. B. Kennel, R. Brown, and H. D. I. Abarbanel, Phys. Rev. A **45**, 3403 (1992).
[14] A. M. Fraser and H. L. Swinney, Phys. Rev. A **33**, 1134 (1986).
[15] H. Nalatore, M. Ding, and G. Rangarajan, Phys. Rev. E **75**, 031123 (2007).
[16] I. I. Mokhov and D. A. Smirnov, Geophys. Res. Lett. **33**, L03708 (2006).
[17] J. Yu, V. A. Smith, P. P. Wang, A. J. Hartemink, and E. D. Jarvis, Bioinformatics **20**, 3594 (2004).
[18] Y. Chen, G. Rangarajan, J. Feng, and M. Ding, Phys. Lett. A **324**, 26 (2004).